Theoretical study on the sabot separation process of a sub-caliber projectile fired from rifled guns

Bui Xuan Son¹, Nguyen Quang Tuan^{1*}, Nguyen Hai Minh¹, Doan Van Dung¹

¹Faculty of Special Equipments, Le Quy Don Technical University, Vietnam.

 $\hbox{**Corresponding author E-mail:} \ \underline{\hbox{tuannguyenmta} 28@gmail.com}$

Received: Jun. 6, 2024 Revised: Jul. 7, 2024 Accepted: Jul. 9, 2024 Online: Jul. 14, 2024

Abstract

Sub-caliber projectiles have been widely used in modern warfare due to their ability to enhance accuracy and ballistic performance. For such projectiles, however, an effective separation of the penetrator from the sabot upon exiting the barrel is extremely important for achieving the desired accuracy and terminal ballistics. In this paper, we present a theoretical model for studying the aspects of the penetrator-sabot separation process for a sub-caliber projectile fired from 7.62mm pistols. The method used in this paper is a combination of analytical and numerical approaches. Firstly, an equation system was analytically established to describe the motion of the sabot and the penetrator in absolute coordinates. Then, the Computational fluid dynamics simulation approach was applied to determine the aerodynamic forces acting on the sabot and the penetrator. Finally, the equation system was solved using Newton's method to calculate the position of the sabot and the penetrator during the separation process. Based on the proposed model, the effect of some parameters on the separation process was investigated. The investigation results have shown that the initial friction force between the sabot and the penetrator significantly influences the separation process. The findings in this study provide valuable contributions to the design and optimization of sub-caliber projectile-weapon systems.

© The Author 2024. Published by ARDA.

Keywords: Sabot separation; sub-caliber projectile; CFD method, armor-piercing power; saboted projectile, penetrator

1. Introduction

To enhance the armor penetration power of projectiles, various solutions have been applied in weapon design practice. One such way is to use sub-caliber projectiles. Central to the functionality of these projectiles is the sabot, a carrier structure that encases the projectile during its initial flight stage before separating to allow the penetrator to continue flying alone towards the intended target.

In Le Quy Don Technical University, an intensive research program has been carried out to find ways to enhance the armor-piercing performance of rifled guns for infantry, focusing on perspective cartridge projectile designs. One of our chosen designs is the design with sabot, the typical structure of which is



presented in Figure 1. The projectile consists of an aluminum sabot and a tungsten carbide penetrator. The penetrator separates from the sabot due to the difference in aerodynamic drags acting on the sabot and the penetrator. The separation begins upon exiting the barrel until the penetrator completely loses mechanical contact with the sabot (Figure 2).

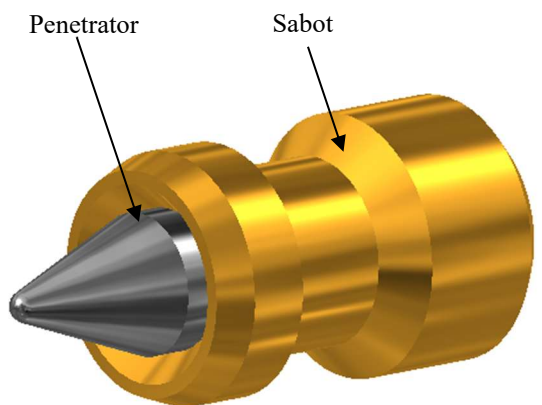


Figure 1. The structure of a sub-caliber projectile fired from rifled guns

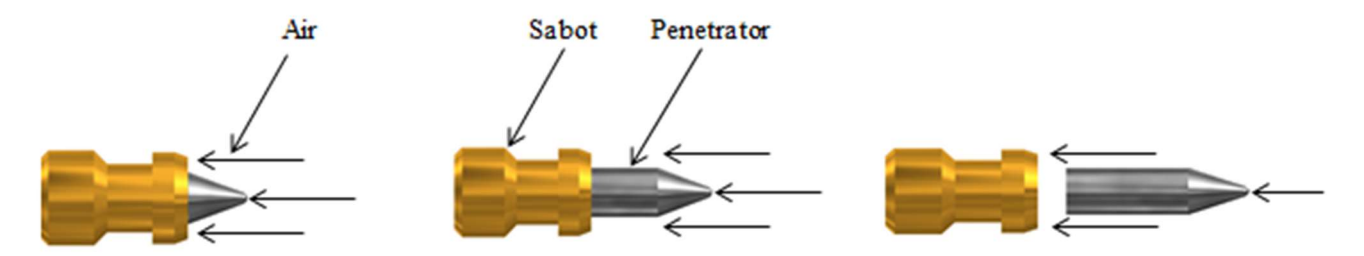


Figure 2. The penetrator gradually separates from the sabot

The penetrator-sabot separation process is an important stage in the flight trajectory of sub-caliber projectiles, influencing their stability, accuracy, and terminal effectiveness. Numerous researches have been conducted on the separation process of APFSDS (Armor-Piercing Fin-Stabilized Discarding Sabot).

Several scholars have carried out experiments to visually observe and analyze the sabot discard process. Others have employed Computational fluid dynamics (CFD) methods to numerically investigate the effect of different parameters, such as muzzle velocity, sabot geometry dimensions, and launch conditions on the separation process [1-5].

The APFSDS projectiles are fired from smoothbore barrels. The penetrator of APFSDS has fins to stabilize its flight. As the APFSDS projectile exits the barrel, the sabot and the penetrator almost immediately lose mechanical contact. The working principle of APFSDS projectiles is different from that of sub-caliber projectiles fired from rifled guns. Consequently, it is inappropriate to apply these research results to the sub-caliber projectiles fired from rifled guns.

Regarding spin-stabilized saboted projectiles, Walling et al. conducted experiments to study the interior and exterior ballistics of a 20 mm saboted penetrator projectile [6]. Nguyen et al. numerically investigated the supersonic flow around a saboted bullet fired from 7.62 mm pistols similar to 6.5x25 mm CBJ APDS rounds [7].

Analysis of the available literature related to saboted projectiles showed that very few works have been devoted to sub-caliber projectiles fired from rifled guns and, to the best of our knowledge, so far there have been no published studies concerning the theoretical study of the motion of spin-stabilize projectiles during the separation process. Hence, the main objective of this paper is to establish a theoretical model to investigate the sabot separation process for sub-caliber projectiles fired from rifled guns, outlining the theoretical framework, mathematical model, and computational method as well.

2. Research methodology

2.1. Equation systems describing the motion of the sabot and the penetrator

To establish a mathematical model describing the motion of the sabot and the penetrator upon exiting the barrel, the following assumptions are implemented:

- The trajectory of the projectile is flat (the gravitational force does not affect its trajectory);
- The angle of attack of the projectile is zero;
- The rotational motion of the projectile does not affect its translational motion.

Let us consider the motion of two material points O_s and O_p respectively under the action of the aerodynamic drags and the friction force between the sabot and the penetrator, where O_s is the center of the cross-section of the sabot bottom surface, and O_p is the center of the cross-section of the penetrator aft surface, as shown in Figure 3.

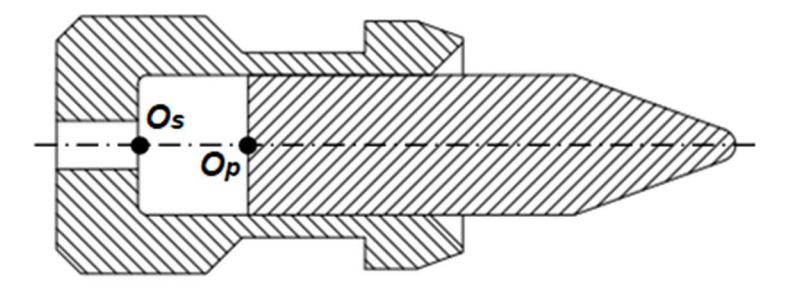


Figure 3. The position of two material points O_s and O_p

A one-dimensional Cartesian coordinate system is next selected for the sabot and the penetrator, as shown in Figure 4.

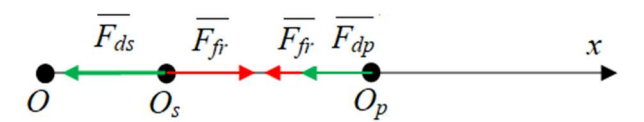


Figure 4. The forces acting on the sabot (O_s) and on the penetrator (O_p)

The origin O of the coordinate system is the center of the cross-section of the penetrator aft surface at the moment the projectile exits the barrel. That means, at the very moment when the projectile exits the barrel, three points O, O_s, and O_p coincide.

The positive direction of the coordinate axis is the direction of the projectile muzzle velocity vector.

According to theoretical physics, the equations describing the motion of the sabot can be stated as follows:

$$\dot{v}_S = \frac{-F_{ds} + F_{fr}}{m_S}$$

$$\dot{x}_S = v_S,$$
(1)

Where v_s is the current velocity of the sabot; x_s is the current coordinate of the sabot; F_{ds} is the aerodynamic drag on the sabot; F_{fr} is the friction between the sabot and the penetrator; m_s is the mass of the sabot. Similarly, the equations describing the motion of the penetrator are as follows:

$$\dot{v}_p = \frac{-F_{dp} - F_{fr}}{m_p}$$

$$\dot{x}_p = v_p,$$
(2)

Where v_p is the current velocity of the penetrator; x_p is the current coordinate of the penetrator; F_{dp} is the aerodynamic drag on the penetrator; and m_p is the mass of the penetrator.

At the initial moment when the projectile is exiting the barrel:

$$v_{s0} = v_{n0} = v_0; x_{s0} = x_{n0} = 0,$$
 (3)

where v_{s0} is the initial velocity of the sabot; v_{p0} is the initial velocity of the penetrator; v_0 is the muzzle velocity of the projectile; x_{s0} is the initial coordinate of the sabot; x_{p0} is the initial coordinate of the penetrator.

The friction between the sabot and the penetrator is determined through the following expression:

$$F_{fr} = f_{fr}pS, (4)$$

where f_{fr} is the friction coefficient between the sabot and the penetrator; p is the specific pressure on the contact surface between the sabot and the penetrator - it depends on the mechanical interference of the sabot and the penetrator; and S is the area of the contact surface between the sabot and the penetrator:

$$S = \pi d_p l, \tag{5}$$

where d_p is the diameter of the penetrator; l is the length of longitudinal contact between the sabot and the penetrator at the current moment as illustrated in Figure 5.

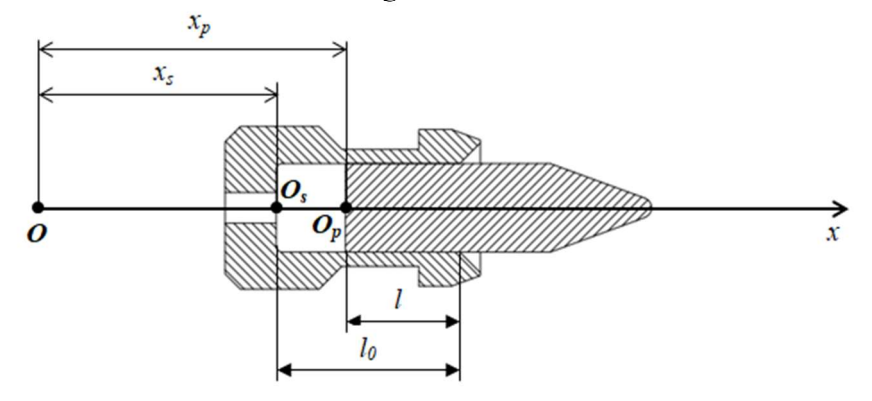


Figure 5. The length of longitudinal contact (1) between the sabot and the penetrator

The parameter l is determined (Fig. 5) as follows:

$$l = l_0 - (x_p - x_s). (6)$$

where l_0 is the initial length of longitudinal contact between the sabot and the penetrator. The separation process is considered to be completed if there is no mechanical contact between the sabot and the penetrator, which means l = 0.

Substituting (5) into (4), we can write:

$$F_{fr} = f_{fr} p \pi d_p l = f_{fr} p \pi d_p l_0 \cdot \frac{l}{l_0}. \tag{7}$$

Naming $F_{fr} = f_{fr}p\pi d_p l_0$, it is easy to realize that F_{fr0} is the initial friction force between the sabot and the penetrator at the very moment when the projectile leaves the gun barrel; it depends on the material properties of the sabot and the penetrator, mechanical interference fit between the sabot and the penetrator, and on the dimensions of the penetrator. Consequently, the expression (7) can be rewritten as follows:

$$F_{fr} = F_{fr} \cdot \frac{l}{l_0}. \tag{8}$$

 $F_{fr} = F_{fr} \cdot \frac{l}{l_0}. \tag{8}$ It is obvious from (8) that the current frictional force between the sabot and the penetrator is linearly dependent on their initial frictional force.

2.2. Solution method

The equation system (1), (2), (6), (8) with initial condition (3) can be solved using numerical methods, if we know the aerodynamic drag F_{ds} and F_{dp} at any time step. To achieve this goal, firstly, these aerodynamic drags are obtained numerically at certain discrete points using the Ansys Fluent software package [8]. Then, F_{ds} and F_{dp} at any time step will be approximated. With fixed dimensions of the sabot and the penetrator, the aerodynamic drags on the sabot and penetrator will depend on their velocity and their relative position. That means they can be presented in the following form:

$$F_{ds} = F_{ds}(v_s, l), \ F_{dp} = F_{dp}(v_p, l). \tag{9}$$

Using numerical simulation method with Ansys Fluent software package we can obtain F_{ds} and F_{dp} at discrete points. To approximate them at any point we use the bilinear interpolation method.

2.3. Procedure for obtaining the aerodynamic drag

In general, aerodynamic drag force can be obtained using semi-empirical prediction codes, like the Missile DATCOM and PRODAS, experimental methods, such as Wind tunnels and Spark Ranges tests, or CFD methods. In this research, we have determined the aerodynamic drag on the sabot and the penetrator using CFD methods with the Ansys Fluent software package. The simulation procedure has been widely presented in multiple works [9-13]. To calculate the aerodynamic drags of the sabot and the penetrator, an air domain with the size of $40D \times 10D \times 10D$ was created, where D is the diameter of the sabot (D = 7.62mm). Mesh sensitivity investigation showed that, in our case, for 3D RANS simulation, the mesh of 3.8 million elements would give sufficiently accurate results. The mesh around the projectile is presented in Figure 6. In order to obtain drag on the sabot and the drag on the penetrator separately, we have named the penetrator surface and the sabot surface with different names as shown in Figure 7. Other setting parameters for Ansys Fluent simulation used in this study are presented in Table 1.



Figure 6. The mesh for the projectile

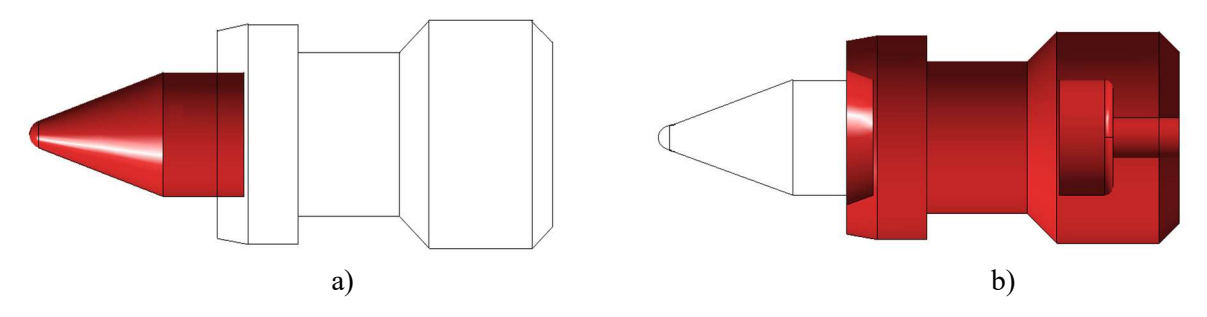


Figure 7. Named selections for the penetrator (a) and the sabot (b)

Table 1. The main setting parameters in Ansys Fluent

Parameter	Value
Turbulence model	k-ε
Solver	Density-based
Air model	Ideal gas
Viscosity model	Sutherland
Algorithm	Coupled
Convergence criteria	10-5

The numerically obtained values of aerodynamic drag on the sabot and the penetrator are presented in Appendix 1 and Appendix 2. To visually observe the supersonic flow in simulation, examples of the flow around the sabot and the penetrator at their velocities and relative positions are presented in Figure 8-11.

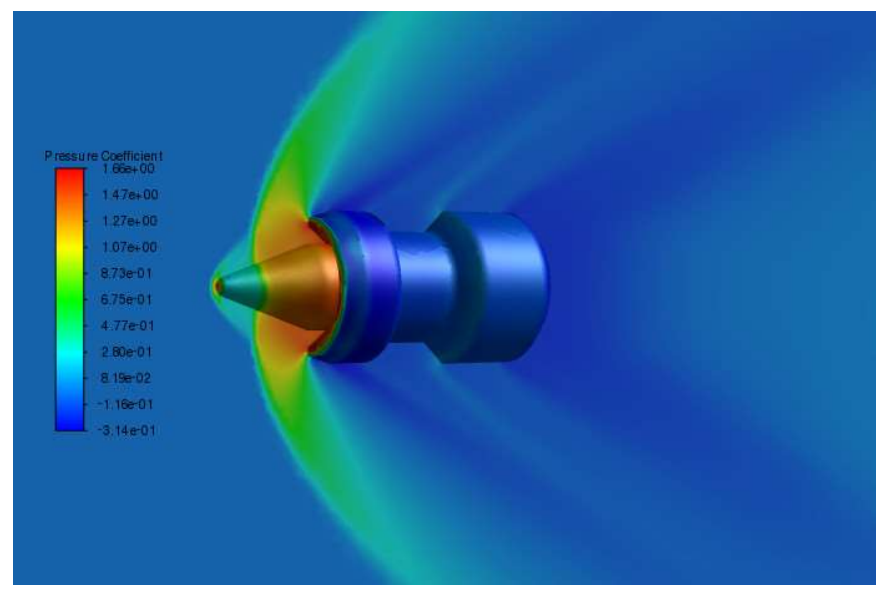


Figure 8. The pressure distribution around the saboted projectile at v = 620 m/s and l = 0 mm

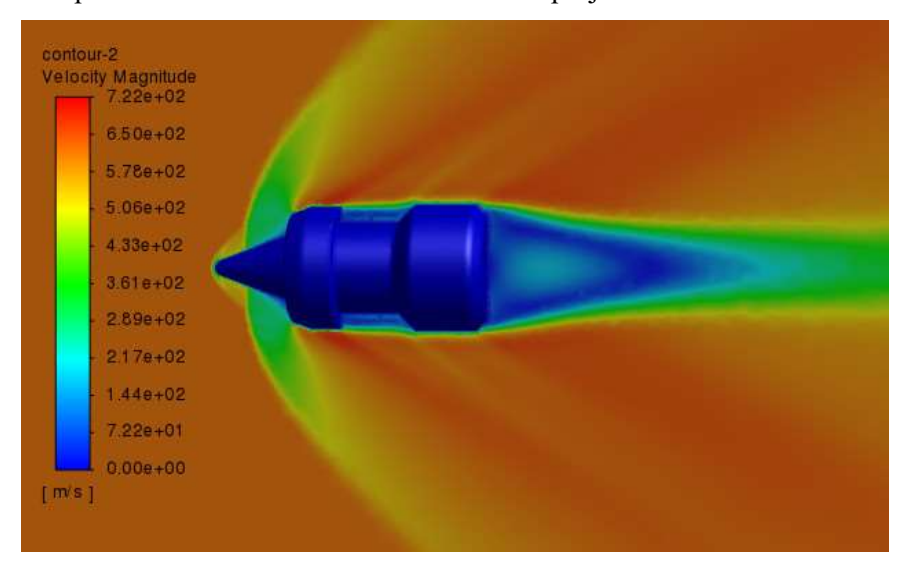


Figure 9. The velocity distribution around the saboted projectile at v = 620 m/s and l = 0 mm

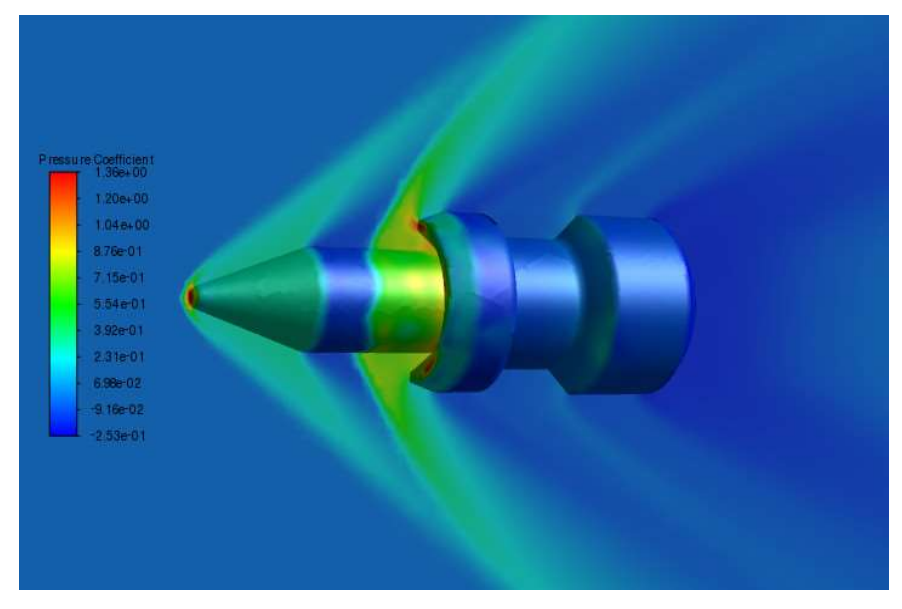


Figure 10. The pressure distribution around the saboted projectile at v = 680 m/s and l = 5 mm

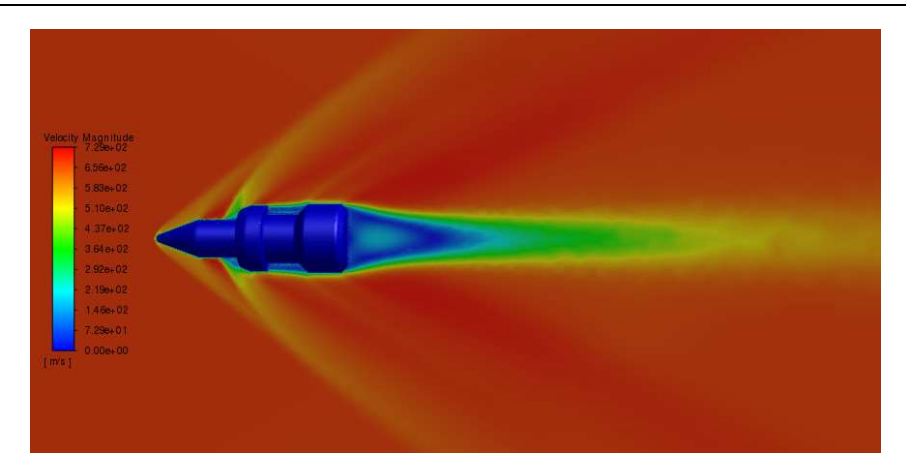


Figure 11. The velocity distribution around the saboted projectile at v = 680 m/s and l = 5 mm

2.4. Approximating the aerodynamic drag

After obtaining the aerodynamic drags on the sabot and the penetrator at discrete points of their velocity and their relative position, we will approximate them at any time step based on their current velocity and relative position using the bilinear interpolation method. Supposing that, using Ansys Fluent simulation software we have obtained aerodynamic drag F at four points $F_{1l}(v_l, l_l)$, $F_{12}(v_l, l_2)$, $F_{2l}(v_2 l_l)$, $F_{22}(v_2, l_2)$. According to the bilinear interpolation method, the value of any F(v, l), where $v_1 < v < v_2$ and $l_1 < l < l_2$, can be approximated by the following expression [14]:

$$F(v,l) = F_{11} + (F_{21} - F_{11}) \frac{v - v_1}{v_2 - v_1} + (F_{12} - F_{11}) \frac{l - l_1}{l_2 - l_1} + (F_{22} - F_{12} - F_{21} + F_{11}) \frac{(v - v_1)(l - l_1)}{(v_2 - v_1)(l_2 - l_1)}.$$

2.5. Result verification

Though the research method has been carefully established, the calculated results should be compared to experimental results to verify the accuracy of the method. As no relevant experimental data has been published in open literature so far, there are some limitations regarding result verification. Nevertheless, the main purpose of this paper is to conduct a theoretical study on the separation process of a saboted projectile; hence, experiments can be carried out later as a further development of this work to verify the comprehensive study model for the separation phenomenon.

3. Results and discussion

The sabot separation process is complex, and influenced by numerous factors, including aerodynamic forces and launch conditions. Understanding these dynamics is crucial for optimizing the accuracy and effectiveness of sub-caliber projectile systems. In this paper, the influence of the muzzle velocity of the projectile and the initial friction between the sabot and the penetrator on the sabot separation process was investigated using above established mathematical model. Namely, we have investigated their influence on the penetrator velocity at the moment it separates from the sabot and on the distance the penetrator travels to the separation point (the separation distance). The main dimensions of the penetrator and the sabot are shown in Figure 12 and Figure 13.

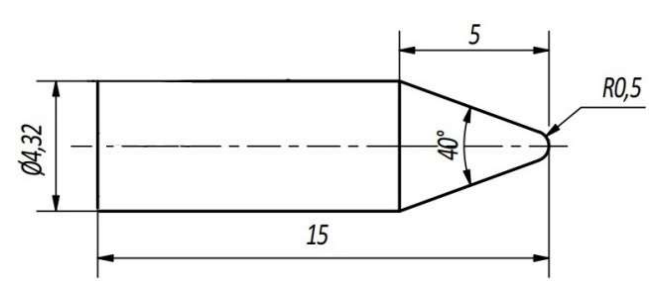


Figure 12. The dimensions of the penetrator

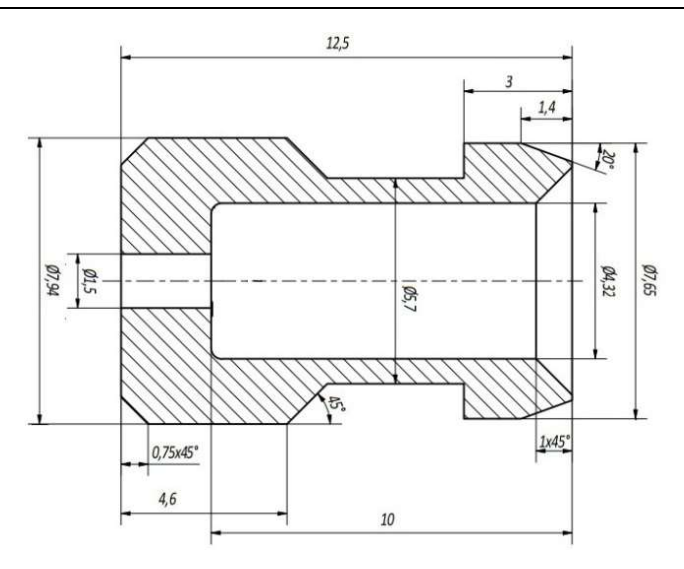


Figure 13. The dimensions of the sabot

In addition, the main parameters of the projectile are presented in Table 2.

rable 2. The main parameters of the sub-canber projectile						
Parameter	Units	Notation	Value			
Mass of the aluminum sabot	kg	m_s	0.00089			
Mass of the tungsten carbide penetrator	kg	m_p	0.00274			
The initial length of longitudinal contact	m	l	0.009			

Table 2. The main parameters of the sub-caliber projectile

Using the Ansys Fluent software package we have obtained aerodynamic drag $F_{ds}(v_s, l)$ and $F_{dp}(v_p, l)$ as discrete functions of their velocity and parameter l: the velocity ranges from 630 m/s to 700 m/s with an increment of 10 m/s, the parameter l changes from 0 m to 0.009 m with an increment of 0.001 m.

A code has been written in Delphi programming language [15] for approximating aerodynamic drags and solving the equation system (1), (2),(6), (8) with initial condition (3) to find the velocity of the projectile at the separation moment and the separation distance. The code is presented in Appendix 3.

3.1. The effect of the projectile muzzle velocity

Projectile muzzle velocity is one of the most important parameters, influencing the trajectory, range, and terminal power of the projectile. In this research, to analyze the effect of the projectile muzzle velocity, we have investigated the sabot separation process with projectile muzzle velocity of 700 m/s, 680 m/s, 660 m/s, and 640 m/s. The influence of the projectile muzzle velocity on the penetrator velocity at the separation moment and on the separation distance is presented in Figure 14 and Figure 15 with different initial friction forces between the sabot and the penetrator.

The dependence of the penetrator velocity at the separation moment on the projectile muzzle velocity is almost linear and nearly identical for different initial friction forces between the sabot and the penetrator (Figure 14). In the contrary, the influence of the projectile muzzle velocity on the separation distance is dependent on the initial friction force between the sabot and the penetrator (Figure 15). The greater the initial friction force the clearer the projectile muzzle velocity affects the separation distance. At the initial friction force of 2 N, the separation distance only slightly changes with the change of the projectile muzzle velocity. But at the initial friction force of 6 N, the projectile muzzle velocity significantly affects the separation distance. Moreover, we can see clearly that, the penetrator completely separates from the sabot at the distance of about 1 m to 1.8 m from the gun muzzle. This information helps us to appropriately setup high-speed camera to capture the separation process for further analysis and development.

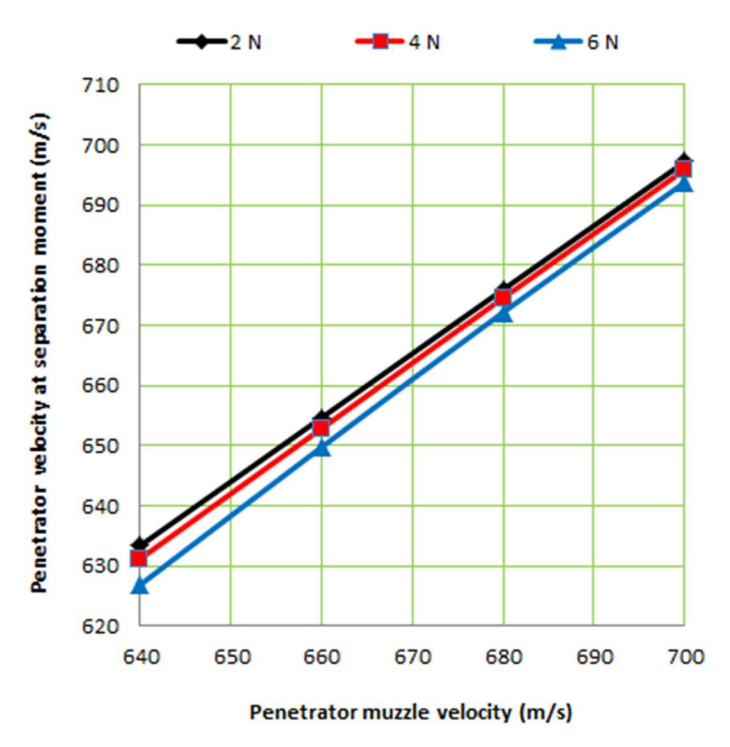


Figure 14. The influence of projectile muzzle velocity on the penetrator velocity at separation moment at different initial friction forces between the sabot and the penetrator

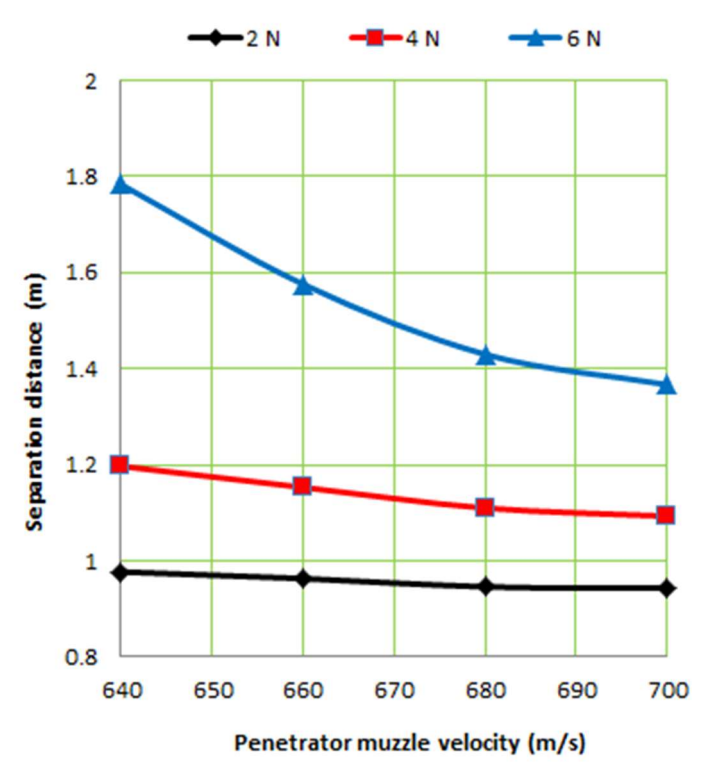


Figure 15. The influence of projectile muzzle velocity on the separation distance at different initial friction forces between the sabot and the penetrator

3.2. The effect of the initial friction force between the sabot and the penetrator

The initial friction force between the sabot and the penetrator is a crucial parameter, affecting the dynamics of the separation process and the transportation, storage, and usage of saboted projectiles. The initial friction force must be appropriately selected to ensure reliable sabot separation, on the one hand, and the integrity of the projectile on the other hand. In this study, the sabot separation process was investigated with initial friction

force from 2 N to 7 N to see its effect. The influence of the initial friction force on the penetrator velocity at the separation moment and on the separation distance is shown in Figure 16 and Figure 17.

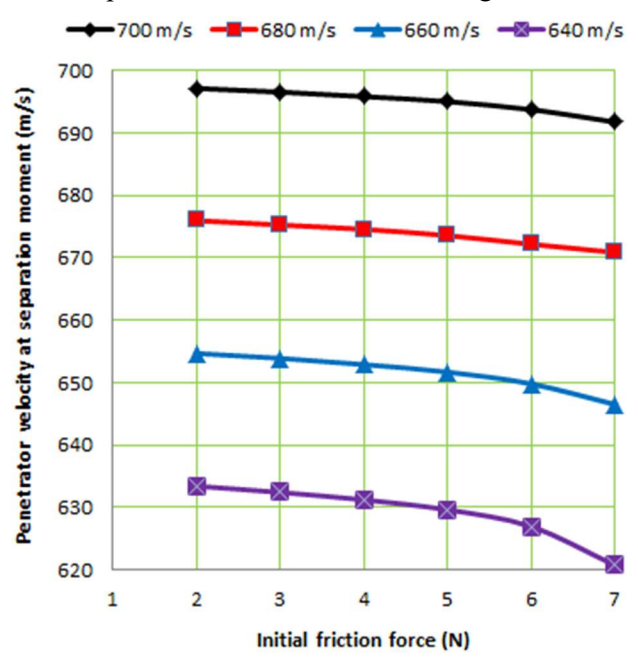


Figure 16. The influence of the initial friction force on the penetrator velocity at separation moment at different projectile muzzle velocities

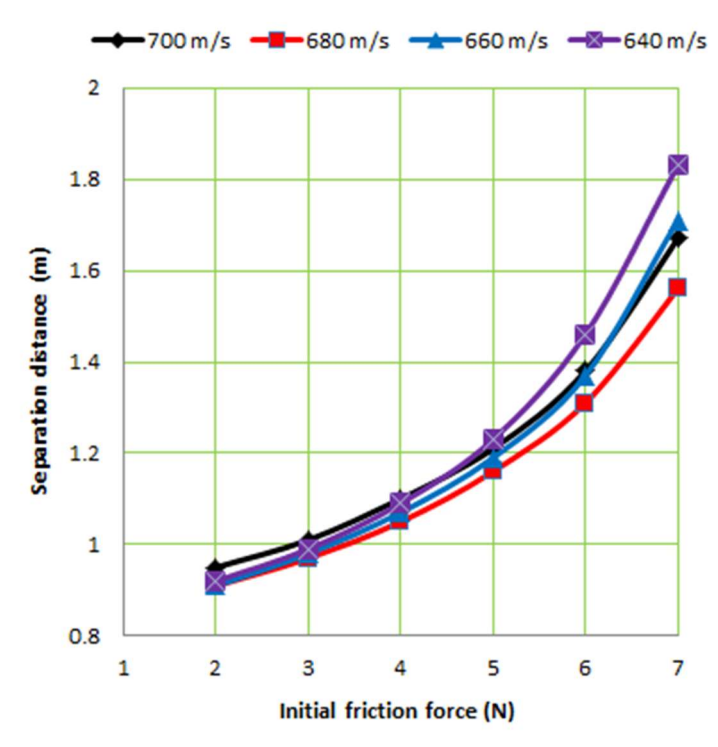


Figure 17. The influence of the initial friction force on the separation distance at different projectile muzzle velocities

It is easy to see that if the initial friction force increases then the penetrator velocity at the separation moment decreases. Moreover, the greater the initial friction force, the more penetrator velocity at the separation moment drops. At an initial friction force of 2 N, the penetrator velocity loss is about 0.4% to 1% depending on the projectile muzzle velocity, while at an initial friction force of 7 N, the penetrator velocity loss is about 0.8% to 2% depending on the projectile muzzle velocity. The greater the projectile muzzle velocity, the less

the penetrator velocity loss. In addition, if the initial friction force increases, the separation distance also increases quickly. At the initial friction force of 2 N, the separation distance is about 1 m, but, at the initial friction force of 7 N, the separation distance is about 1.6 m to 1.8 m.

Thus, it can be affirmed that the initial friction force between the sabot and the penetrator has a very significant influence on the decrease of the penetrator velocity at the time it completely separates from the sabot, and also on the separation distance. In the process of designing and manufacturing saboted projectiles, it is necessary to select the initial friction force appropriately to ensure that the penetrator connects reliably with the sabot during transportation, storage, and reloading and that the penetrator can reliably and promptly separate from the sabot after the projectile exiting the gun barrel. In this case, the initial friction force should be between 3 N and 7 N to ensure a reliable connection between the sabot and the penetrator and ensure that the separation process occurs beyond the aftereffect period of gunpowder gas.

4. Conclusions

In this research, a theoretical model was proposed for studying the sabot separation process of a sub-caliber projectile fired from rifled guns. Based on this model, an investigation was conducted to analyze the effect of the initial friction force between the sabot and the penetrator and the effect of the projectile muzzle velocity on the separation process. The results have shown a significant influence of the initial friction force on the penetrator velocity at the separation moment and on the separation distance. The separation distance varies from about 1 m to 1.8 m. The appropriate initial friction force between the sabot and the penetrator should be from 3 N to 7 N. The research methodology and results presented in this study can be applied in the design process to enhance the effectiveness of saboted projectile-weapon systems.

5. Future work

The following directions are recommended for further continuation of this study:

- 1. The first direction is to investigate the influence of the structural parameters of the sabot on the separation process.
- 2. The second direction is to numerically investigate the sabot separation process of sub-caliber projectiles fired from a rifled gun using the Fluid-structure interaction (FSI) approach and then compare the obtained results with the results of this study.
- 3. The third direction is to conduct live firing tests to verify and validate the reliability and accuracy of the established mathematical model and computational method.

Funding information

This research received no specific grant from any funding agency in the public, commercial, or not-for-profit sectors.

Declaration of competing interest

The authors declare that they have no known competing financial interests or personal relationships that could have appeared to influence the work reported in this paper.

References

- [1] C. Zhang, H. Wang, T. Liu, and Y. Duo, "Sabot discard characteristics under different spin rates of the rifled barrel launching APFSDS," *Shock and Vibration*, vol. 2021, 2021.
- [2] R. Cayzac, E. Carette, and S. Heddadj, "Complex aerodynamics behavior of high spin APFSDS projectile," *International Journal of Applied Mechanics*, vol. 80, no. 3, pp. 1-7, 2013.
- [3] Z. Hoang and Z. Chen, "Numerical simulation on three-dimensional dynamic process of sabot discarding of APFSDS," *Acta Armamentarii*, vol. 35, no. 1, pp. 9-17, 2014.

- [4] L. Huang and C. Lai, "Systematic study and numerical simulation of sabot projectile aerodynamics," *Journal of the Chinese Institute of Engineers*, vol. 20, no. 3, pp. 275-284, 1997.
- [5] A. Trakic, "Axial force coefficient of APFSDS projectile," *Defense and Security Studies*, vol. 1, pp. 1-15, 2020.
- [6] H. C. Walling, T. J. Roemer, and K. Svensson, "Interior and exterior ballistic development of a 20mm saboted penetrator projectile," *Sandia National Laboratories*, 1997.
- [7] Q. T. Nguyen, H. M. Nguyen, and X. S. Bui, "Numerical investigation on the supersonic flow around a saboted bullet," *Military Technical Courier*, vol. 72, no. 2, pp. 676-694, 2024.
- [8] J. E. Matsson, An Introduction to Ansys Fluent 2023, SDC Publications, 2023.
- [9] A. Catovic and E. Kljuno, "Prediction of aerodynamic coefficients for the irregularly shaped body using numerical simulations," *International Journal of Advanced and Applied Sciences*, vol. 5, no. 7, pp. 71-85, 2018.
- [10] A. Ferfouri, T. Allouche, D. D. Jerkovic, N. Hristov, M. Vuckovic, and A. Benmeddah, "Prediction of drag aerodynamic coefficient of the 155 mm projectile under axisymmetric flow using different approaches," *Journal of the Serbian Society for Computational Mechanics*, vol. 17, no. 2, pp. 69-86, 2023.
- [11] A. Khan, I. Shah, A. Aziz, M. Waqas, U. K. Zaman, and D. Jung, "Numerical and experimental analysis of drag and lift forces on a bullet head," *Aerospace*, vol. 9, pp. 1-16, 2022.
- [12] Q. Hao, Q. Jiang, C. Xu, and L. Liu, "Aerodynamic characterization of bullet heads with different accurate curves," *Journal of Applied Fluid Mechanics*, vol. 17, no. 5, pp. 1015-1026, 2024.
- [13] T. Sabanovic, "Analysis of the influence of 5.56 mm projectile shape on drag coefficient using CFD," *Defense and Security Studies*, vol. 2, pp. 79-85, 2021.
- [14] H. R. Kang, Computational Color Technology, Society of Photo Optical, 2006.
- [15] J. Barrow, L. Miller, K. Malan, and H. Gelderblom, Introducing Delphi Programming: Theory through Practice, 4th ed., Oxford University Press, 2005.

Appendix 1. The aerodynamic drag on the sabot, obtained using Ansys Fluent

					$F_{ds}(N)$					
l (m)	0	0.001	0.002	0.003	0.004	0.005	0.006	0.007	0.008	0.009
v(m/s)										
700	12.40	13.00	10.41	10.76	9.46	9.19	9.74	9.46	9.64	9.23
690	12.07	12.49	10.19	10.49	9.15	8.96	9.45	9.12	9.38	9.08
680	11.78	12.03	10.01	10.27	8.83	8.67	9.13	8.66	9.15	8.96
670	11.37	11.72	9.78	10.01	8.75	8.35	8.90	8.56	9.01	8.84
660	10.98	11.29	9.58	9.70	8.64	8.06	8.62	8.40	8.83	8.78
650	10.72	10.84	9.45	9.48	8.48	7.98	8.44	8.18	8.60	8.57
640	10.26	10.58	9.11	9.43	8.34	7.95	8.24	8.02	8.32	8.30
630	9.78	10.15	8.93	9.01	8.23	7.73	7.98	7.68	7.97	8.02

Appendix 2. The aerodynamic drag on the penetrator, obtained using Ansys Fluent

$F_{dp}(N)$										
l (m) v(m/s)	0	0.001	0.002	0.003	0.004	0.005	0.006	0.007	0.008	0.009
700	4.23	2.64	1.45	1.46	1.47	1.48	1.49	1.51	1.52	1.53
690	4.14	2.61	1.42	1.43	1.43	1.44	1.45	1.47	1.48	1.49
680	4.09	2.59	1.39	1.40	1.41	1.41	1.42	1.44	1.45	1.46
670	4.07	2.55	1.36	1.37	1.37	1.38	1.38	1.40	1.42	1.43
660	3.93	2.49	1.33	1.34	1.34	1.35	1.35	1.37	1.38	1.40
650	3.86	2.47	1.28	1.30	1.31	1.31	1.32	1.34	1.35	1.36
640	3.74	2.44	1.26	1.27	1.28	1.28	1.29	1.32	1.32	1.33
630	3.63	2.41	1.23	1.24	1.25	1.25	1.26	1.27	1.27	1.28

Appendix 3. The code, written in Delphi programming language for approximating aerodynamic drags and solving the equations of motion of the sabot and the penetrator unit Unit1; interface uses Winapi.Windows, Winapi.Messages, System.SysUtils, System.Variants, System.Classes, Vcl.Graphics, Vcl.Controls, Vcl.Forms, Vcl.Dialogs, Vcl.StdCtrls; implementation {\$R *.dfm} {Input of the initial structural parameters} procedure TForm1.Button3Click(Sender: TObject); begin Edit1.Text:='9'; Edit2.Text:='2'; Edit5.Text:="; Edit7.Text:="; Edit8.Text:='0.89'; Edit9.Text:='2.74'; Edit10.Text:='690'; Edit11.Text:='0.0000001'; Edit12.Text:="; Edit13.Text:="; end; procedure Input1; begin 10:=StrToFloat(form1.Edit1.Text)/1000; Ffr0:=StrToFloat(form1.Edit2.Text); ms:=StrToFloat(form1.Edit8.Text)/1000; mp:=StrToFloat(form1.Edit9.Text)/1000; v0:=StrToFloat(form1.Edit10.Text); step:=StrToFloat(form1.Edit11.Text); end; {Input of the aerodynamic drags obtained from Ansys Fluent} procedure Input2; begin vs0[1]:=700; vs0[2]:=690; vs0[3]:=680; vs0[4]:=670; vs0[5]:=660; vs0[6]:=650; vs0[7]:=640; vs0[8]:=630; vp0[1]:=700; vp0[2]:=690; vp0[3]:=680; vp0[4]:=670; vp0[5]:=660; vp0[6]:=650; vp0[7]:=640; vp0[8]:=630; 110[1]:=0; 110[2]:=1; 110[3]:=2; 110[4]:=3; 110[5]:=4; 110[6]:=5; 110[7]:=6; 110[8]:=7; 110[9]:=8; 110[10]:=9;Fds0[1,1]:=12.40; Fds0[1,2]:=13.00; Fds0[1,3]:=10.41; Fds0[1,4]:=10.76; Fds0[1,5]:=9.46; Fds0[1,6]:=9.19; Fds0[1,7]:=9.74; Fds0[1,8]:=9.46; Fds0[1,9]:=9.64; Fds0[1,10]:=9.23; Fds0[2,1]:=12.07; Fds0[2,2]:=12.49; Fds0[2,3]:=10.19; Fds0[2,4]:=10.49; Fds0[2,5]:=9.15; Fds0[2,6]:=8.96; Fds0[2,7]:=9.45; Fds0[2,8]:=9.12; Fds0[2,9]:=9.38; Fds0[2,10]:=9.08; Fds0[3,1]:=11.78; Fds0[3,2]:=12.03; Fds0[3,3]:=10.01; Fds0[3,4]:=10.27; Fds0[3,5]:=8.83; Fds0[3,6]:=8.67; Fds0[3,7]:=9.13; Fds0[3,8]:=8.66; Fds0[3,9]:=9.15; Fds0[3,10]:=8.96; Fds0[4,1]:=11.37; Fds0[4,2]:=11.72; Fds0[4,3]:=9.78; Fds0[4,4]:=10.01; Fds0[4,5]:=8.75; Fds0[4,6]:=8.35; Fds0[4,7]:=8.90; Fds0[4,8]:=8.56; Fds0[4,9]:=9.01; Fds0[4,10]:=8.84; Fds0[5,1]:=10.98; Fds0[5,2]:=11.29; Fds0[5,3]:=9.58; Fds0[5,4]:=9.70; Fds0[5,5]:=8.64; Fds0[5,6]:=8.06; Fds0[5,7]:=8.62; Fds0[5,8]:=8.40; Fds0[5,9]:=8.83; Fds0[5,10]:=8.78; Fds0[6,1]:=10.72; Fds0[6,2]:=10.84; Fds0[6,3]:=9.45; Fds0[6,4]:=9.48; Fds0[6,5]:=8.48; Fds0[6,6]:=7.98; Fds0[6,7]:=8.44; Fds0[6,8]:=8.18; Fds0[6,9]:=8.60; Fds0[6,10]:=8.57;

Fds0[7,1]:=10.26; Fds0[7,2]:=10.58; Fds0[7,3]:=9.11; Fds0[7,4]:=9.43; Fds0[7,5]:=8.34; Fds0[7,6]:=7.95;

Fds0[8,1]:=9.78; Fds0[8,2]:=10.15; Fds0[8,3]:=8.93; Fds0[8,4]:=9.01; Fds0[8,5]:=8.23; Fds0[8,6]:=7.73;

Fds0[7,7]:=8.24; Fds0[7,8]:=8.02; Fds0[7,9]:=8.32; Fds0[7,10]:=8.30;

Fds0[8,7]:=7.98; Fds0[8,8]:=7.68; Fds0[8,9]:=7.97; Fds0[8,10]:=8.02;

```
Fdp0[1,1]:=4.23; Fdp0[1,2]:=2.64; Fdp0[1,3]:=1.45; Fdp0[1,4]:=1.46; Fdp0[1,5]:=1.47; Fdp0[1,6]:=1.48;
Fdp0[1,7]:=1.49; Fdp0[1,8]:=1.51; Fdp0[1,9]:=1.52; Fdp0[1,10]:=1.53;
Fdp0[2,1]:=4.14; Fdp0[2,2]:=2.61; Fdp0[2,3]:=1.42; Fdp0[2,4]:=1.43; Fdp0[2,5]:=1.43; Fdp0[2,6]:=1.44;
Fdp0[2,7]:=1.45; Fdp0[2,8]:=1.47; Fdp0[2,9]:=1.48; Fdp0[2,10]:=1.49;
Fdp0[3,1]:=4.09; Fdp0[3,2]:=2.59; Fdp0[3,3]:=1.39; Fdp0[3,4]:=1.40; Fdp0[3,5]:=1.41; Fdp0[3,6]:=1.41;
Fdp0[3,7]:=1.42; Fdp0[3,8]:=1.44; Fdp0[3,9]:=1.45; Fdp0[3,10]:=1.46;
Fdp0[4,1]:=4.07; Fdp0[4,2]:=2.55; Fdp0[4,3]:=1.36; Fdp0[4,4]:=1.37; Fdp0[4,5]:=1.37; Fdp0[4,6]:=1.38;
Fdp0[4,7]:=1.38; Fdp0[4,8]:=1.40; Fdp0[4,9]:=1.42; Fdp0[4,10]:=1.43;
Fdp0[5,1]:=3.93; Fdp0[5,2]:=2.49; Fdp0[5,3]:=1.33; Fdp0[5,4]:=1.34; Fdp0[5,5]:=1.34; Fdp0[5,6]:=1.35;
Fdp0[5,7]:=1.35; Fdp0[5,8]:=1.37; Fdp0[5,9]:=1.38; Fdp0[5,10]:=1.40;
Fdp0[6,1]:=3.86; Fdp0[6,2]:=2.47; Fdp0[6,3]:=1.28; Fdp0[6,4]:=1.30; Fdp0[6,5]:=1.31; Fdp0[6,6]:=1.31;
Fdp0[6,7]:=1.32; Fdp0[6,8]:=1.34; Fdp0[6,9]:=1.35; Fdp0[6,10]:=1.36;
Fdp0[7,1]:=3.74; Fdp0[7,2]:=2.44; Fdp0[7,3]:=1.26; Fdp0[7,4]:=1.27; Fdp0[7,5]:=1.28; Fdp0[7,6]:=1.28;
Fdp0[7,7]:=1.29; Fdp0[7,8]:=1.32; Fdp0[7,9]:=1.32; Fdp0[7,10]:=1.33;
Fdp0[8,1]:=3.63; Fdp0[8,2]:=2.41; Fdp0[8,3]:=1.23; Fdp0[8,4]:=1.24; Fdp0[8,5]:=1.25; Fdp0[8,6]:=1.25;
Fdp0[8,7]:=1.26; Fdp0[8,8]:=1.27; Fdp0[8,9]:=1.27; Fdp0[8,10]:=1.28;
  end;
                                              {Approximating the aerodynamic drag on the sabot}
Function Fds(a,b:real):real;
var x,y:integer;
F11,F12,F21,F22:real;
begin
if (a \le 700) and (a \ge 690) then x = 1; if (a \le 690) and (a \ge 680) then x = 2; if (a \le 680) and (a \ge 670) then x = 3;
if (a \le 670) and (a \ge 660) then x = 4; if (a \le 660) and (a \ge 650) then x = 5; if (a \le 650) and (a \ge 640) then x = 6;
if (a \le 640) and (a \ge 630) then x = 7;
if (b<1) and (b>=0) then y:=1; if (b<2) and (b>=1) then y:=2; if (b<3) and (b>=2) then y:=3;
if (b<4) and (b>=3) then y:=4; if (b<5) and (b>=4) then y:=5; if (b<6) and (b>=5) then y:=6;
if (b<7) and (b>=6) then y:=7; if (b<8) and (b>=7) then y:=8; if (b<9) and (b>=8) then y:=9;
F11:=Fds0[x,y]; F12:=Fds0[x,y+1]; F21:=Fds0[x+1,y]; F22:=Fds0[x+1,y+1];
Fds:=F11+(F21-F11)*(a-vs0[x])/(vs0[x+1]-vs0[x])+(F12-F11)*(b-ll0[x])/(ll0[x+1]-ll0[x])+(F22-F12-ll0[x])+(F22-F12-ll0[x])+(F22-F12-ll0[x])+(F22-F12-ll0[x])+(F22-F12-ll0[x])+(F22-F12-ll0[x])+(F22-F12-ll0[x])+(F22-F12-ll0[x])+(F22-F12-ll0[x])+(F22-F12-ll0[x])+(F22-F12-ll0[x])+(F22-F12-ll0[x])+(F22-F12-ll0[x])+(F22-F12-ll0[x])+(F22-F12-ll0[x])+(F22-F12-ll0[x])+(F22-F12-ll0[x])+(F22-F12-ll0[x])+(F22-F12-ll0[x])+(F22-F12-ll0[x])+(F22-F12-ll0[x])+(F22-F12-ll0[x])+(F22-F12-ll0[x])+(F22-F12-ll0[x])+(F22-F12-ll0[x])+(F22-F12-ll0[x])+(F22-F12-ll0[x])+(F22-F12-ll0[x])+(F22-F12-ll0[x])+(F22-F12-ll0[x])+(F22-F12-ll0[x])+(F22-F12-ll0[x])+(F22-F12-ll0[x])+(F22-F12-ll0[x])+(F22-F12-ll0[x])+(F22-F12-ll0[x])+(F22-F12-ll0[x])+(F22-F12-ll0[x])+(F22-F12-ll0[x])+(F22-F12-ll0[x])+(F22-F12-ll0[x])+(F22-F12-ll0[x])+(F22-F12-ll0[x])+(F22-F12-ll0[x])+(F22-F12-ll0[x])+(F22-F12-ll0[x])+(F22-F12-ll0[x])+(F22-F12-ll0[x])+(F22-F12-ll0[x])+(F22-F12-ll0[x])+(F22-F12-ll0[x])+(F22-F12-ll0[x])+(F22-F12-ll0[x])+(F22-F12-ll0[x])+(F22-F12-ll0[x])+(F22-F12-ll0[x])+(F22-F12-ll0[x])+(F22-F12-ll0[x])+(F22-F12-ll0[x])+(F22-F12-ll0[x])+(F22-F12-ll0[x])+(F22-F12-ll0[x])+(F22-F12-ll0[x])+(F22-F12-ll0[x])+(F22-F12-ll0[x])+(F22-F12-ll0[x])+(F22-F12-ll0[x])+(F22-F12-ll0[x])+(F22-F12-ll0[x])+(F22-F12-ll0[x])+(F22-F12-ll0[x])+(F22-F12-ll0[x])+(F22-F12-ll0[x])+(F22-F12-ll0[x])+(F22-F12-ll0[x])+(F22-F12-ll0[x])+(F22-F12-ll0[x])+(F22-F12-ll0[x])+(F22-F12-ll0[x])+(F22-F12-ll0[x])+(F22-F12-ll0[x])+(F22-F12-ll0[x])+(F22-F12-ll0[x])+(F22-F12-ll0[x])+(F22-F12-ll0[x])+(F22-F12-ll0[x])+(F22-F12-ll0[x])+(F22-F12-ll0[x])+(F22-F12-ll0[x])+(F22-F12-ll0[x])+(F22-F12-ll0[x])+(F22-F12-ll0[x])+(F22-F12-ll0[x])+(F22-F12-ll0[x])+(F22-F12-ll0[x])+(F22-F12-ll0[x])+(F22-F12-ll0[x])+(F22-F12-ll0[x])+(F22-F12-ll0[x])+(F22-F12-ll0[x])+(F22-F12-ll0[x])+(F22-F12-ll0[x])+(F22-F12-ll0[x])+(F22-F12-ll0[x])+(F22-F12-ll0[x])+(F22-F12-ll0[x])+(F22-F12-ll0[x])+(F22-F12-ll0[x])+(F22-F12-ll0[x])+(F22-F12-ll0[x])+(F22-F12-ll0[x])+(F22-ll0[x])+(F22-ll0[x])+(F22-ll0[x])+(F22-ll0[x])+(F22-ll0[x])+(F22-
F21+F11)*(a-vs0[x])/(vs0[x+1]-vs0[x])*(b-ll0[x])/(ll0[x+1]-ll0[x])
end;
                                          {Approximating the aerodynamic drag on the penetrator}
Function Fdp(a,b:real):real;
var x,y:integer;
F11,F12,F21,F22:real;
begin
if (a \le 700) and (a \ge 690) then x = 1; if (a \le 690) and (a \ge 680) then x = 2; if (a \le 680) and (a \ge 670) then x = 3;
if (a\leq=670) and (a\geq660) then x:=4; if (a\leq=660) and (a\geq650) then x:=5; if (a\leq=650) and (a\geq640) then x:=6;
if (a \le 640) and (a \ge 630) then x = 7;
if (b<1) and (b>=0) then y:=1; if (b<2) and (b>=1) then y:=2; if (b<3) and (b>=2) then y:=3;
if (b<4) and (b>=3) then y:=4; if (b<5) and (b>=4) then y:=5; if (b<6) and (b>=5) then y:=6;
 if (b<7) and (b>=6) then y:=7; if (b<8) and (b>=7) then y:=8; if (b<9) and (b>=8) then y:=9;
F11:=Fdp0[x,y]; F12:=Fdp0[x,y+1]; F21:=Fdp0[x+1,y]; F22:=Fdp0[x+1,y+1];
```

```
Fdp:=F11+(F21-F11)*(a-vp0[x])/(vp0[x+1]-vp0[x])+(F12-F11)*(b-l10[x])/(l10[x+1]-l10[x])+(F22-F12-l10[x])+(F22-F12-l10[x])+(F22-F12-l10[x])+(F22-F12-l10[x])+(F22-F12-l10[x])+(F22-F12-l10[x])+(F22-F12-l10[x])+(F22-F12-l10[x])+(F22-F12-l10[x])+(F22-F12-l10[x])+(F22-F12-l10[x])+(F22-F12-l10[x])+(F22-F12-l10[x])+(F22-F12-l10[x])+(F22-F12-l10[x])+(F22-F12-l10[x])+(F22-F12-l10[x])+(F22-F12-l10[x])+(F22-F12-l10[x])+(F22-F12-l10[x])+(F22-F12-l10[x])+(F22-F12-l10[x])+(F22-F12-l10[x])+(F22-F12-l10[x])+(F22-F12-l10[x])+(F22-F12-l10[x])+(F22-F12-l10[x])+(F22-F12-l10[x])+(F22-F12-l10[x])+(F22-F12-l10[x])+(F22-F12-l10[x])+(F22-F12-l10[x])+(F22-F12-l10[x])+(F22-F12-l10[x])+(F22-F12-l10[x])+(F22-F12-l10[x])+(F22-F12-l10[x])+(F22-F12-l10[x])+(F22-F12-l10[x])+(F22-F12-l10[x])+(F22-F12-l10[x])+(F22-F12-l10[x])+(F22-F12-l10[x])+(F22-F12-l10[x])+(F22-F12-l10[x])+(F22-F12-l10[x])+(F22-F12-l10[x])+(F22-F12-l10[x])+(F22-F12-l10[x])+(F22-F12-l10[x])+(F22-F12-l10[x])+(F22-F12-l10[x])+(F22-F12-l10[x])+(F22-F12-l10[x])+(F22-F12-l10[x])+(F22-F12-l10[x])+(F22-F12-l10[x])+(F22-F12-l10[x])+(F22-F12-l10[x])+(F22-F12-l10[x])+(F22-F12-l10[x])+(F22-F12-l10[x])+(F22-F12-l10[x])+(F22-F12-l10[x])+(F22-F12-l10[x])+(F22-F12-l10[x])+(F22-F12-l10[x])+(F22-F12-l10[x])+(F22-F12-l10[x])+(F22-F12-l10[x])+(F22-F12-l10[x])+(F22-F12-l10[x])+(F22-F12-l10[x])+(F22-F12-l10[x])+(F22-F12-l10[x])+(F22-F12-l10[x])+(F22-F12-l10[x])+(F22-F12-l10[x])+(F22-F12-l10[x])+(F22-F12-l10[x])+(F22-F12-l10[x])+(F22-F12-l10[x])+(F22-F12-l10[x])+(F22-F12-l10[x])+(F22-F12-l10[x])+(F22-F12-l10[x])+(F22-F12-l10[x])+(F22-F12-l10[x])+(F22-F12-l10[x])+(F22-F12-l10[x])+(F22-F12-l10[x])+(F22-F12-l10[x])+(F22-F12-l10[x])+(F22-F12-l10[x])+(F22-F12-l10[x])+(F22-F12-l10[x])+(F22-F12-l10[x])+(F22-F12-l10[x])+(F22-F12-l10[x])+(F22-F12-l10[x])+(F22-F12-l10[x])+(F22-F12-l10[x])+(F22-F12-l10[x])+(F22-F12-l10[x])+(F22-F12-l10[x])+(F22-F12-l10[x])+(F22-F12-l10[x])+(F22-F12-l10[x])+(F22-F12-l10[x])+(F22-F12-l10[x])+(F22-F12-l10[x])+(F22-F12-l10[x])+(F22-F12-l10[x])+(F22-F12-l10[x])+(F22-F12-l10[x])+(F
F21+F11)*(a-vp0[x])/(vp0[x+1]-vp0[x])*(b-ll0[x])/(ll0[x+1]-ll0[x]);
 end;
                                                                              {Solving the equations of motion of the sabot and the penetrator}
procedure TForm1.Button1Click(Sender: TObject);
 var
 t,vs,xs,vp,xp,l,Ffr:real;
begin
 Input1; Input2;
 t = 0;
 vs:=v0;
 vp:=v0;
 xs = 0;
 xp:=0;
 1:=0;
 Ffr:=Ffr0;
 Repeat
     t:=t+step;
     vs:=(-Fds(vs,l)+Ffr)/ms*step+vs;
      vp:=(-Fdp(vp,l)-Ffr)/mp*step+vp;
      xs:=vs*step+xs;
      xp:=vp*step+xp;
     1:=(xp-xs);
     Ffr:=Ffr0*(1-1/10);
 Until abs(1-10)<=0.00001;
 form1.Edit5.Text:=FloatToStrF(xp,ffFixed, 16, 2);
 form1.Edit7.Text:=FloatToStrF(vp,ffFixed, 16, 2);
 form1.Edit12.Text:=FloatToStrF(vs,ffFixed, 16, 2);
 form1.Edit13.Text:=FloatToStrF(t,ffFixed, 16, 4);
end;
end.
```